scientific reports

Check for updates

OPEN

Drone-based microclimate analytics reveal vegetation–shade interaction as a key environmental drivers of *Aedes*-prone microhabitat suitability

Zulfadli Mahfodz[1], Agus Naba[2], Siti Aekbal Salleh[3], Pradeep Isawasan[4], Mohd Azuraidi Osman[5] & Nazri Che Dom[1,2,3,6]✉

Urban microclimate interactions between vegetation and shading play a critical role in shaping environmental conditions that influence mosquito habitat suitability in tropical cities. This study presents a drone-based analytical framework to map fine-scale *Aedes*-prone microhabitats across contrasting urban morphologies in Shah Alam, Malaysia. High-resolution UAV imagery was used to quantify vegetation and shading patterns and integrate them into a composite ecological risk model to identify micro-environmental conditions associated with Aedes habitat suitability. Terrace housing exhibited substantially higher ecological risk compared with high-rise forms, reflecting differences in vegetation density and spatial configuration. Statistical modelling suggested that the interaction between vegetation and shading significantly improved predictive performance, highlighting their combined influence on habitat suitability. Spatial analyses further identified persistent shaded zones associated with building orientation and vegetation adjacency, indicating localized micro-environments conducive to mosquito persistence. These findings highlight a critical trade-off in urban design, where greening strategies may inadvertently support mosquito survival if not properly managed. The proposed framework provides a scalable and data-driven approach for identifying high-risk microhabitats and supports its integration into a promising complementary tool for precision surveillance, urban planning, and climate-sensitive public health strategies.

Keywords Urban microclimate, UAV analytics, Vegetation–shade coupling, *Aedes* ecology, Tropical resilience, Climate-sensitive health planning

Dengue fever remains one of the most pervasive vector-borne diseases worldwide, infecting an estimated 390 million people annually, with Southeast Asia accounting for nearly 70% of the global burden[1,2]. In Malaysia, dengue incidence continues to escalate despite decades of vector-control programs, with Selangor consistently recording the highest case numbers[3]. This persistent transmission reflects an underlying limitation in how mosquito habitats are monitored and understood within rapidly urbanizing environments. Conventional surveillance methods; larval surveys, ovitrap indices, and field inspections are labour-intensive, spatially biased, and reactive. They capture breeding foci only after outbreaks emerge, offering little predictive value[4]. Yet the ecological drivers of *Aedes* proliferation, including vegetation density, shade persistence, and humidity, vary at fine spatial scales that traditional tools cannot capture[5,6]. To close this gap, computational geospatial approaches

[1]Centre of Environmental Health & Safety, Faculty of Health Sciences, Universiti Teknologi MARA (UiTM), UITM Selangor, Puncak Alam 42300, Selangor, Malaysia. [2]Department of Physics, University of Brawijaya, Veteren Street, Malang 65145, Indonesia. [3]Institute of Biodiversity and Sustainable Development, Universiti Teknologi Mara (UiTM), Shah Alam 40450, Selangor, Malaysia. [4]Faculty of Computer and Mathematical Sciences, Universiti Teknologi MARA, UITM Perak, Shah Alam 35400, Perak, Malaysia. [5]Department of Cell and Molecular Biology, Faculty of Biotechnology & Biomolecular Sciences, Universiti Putra Malaysia, Serdang 43400, Selangor, Malaysia. [6]Faculty of Health Sciences, Universiti Teknologi MARA, UITM Selangor, Puncak Alam 42300, Selangor, Malaysia. ✉email: nazricd@uitm.edu.my

are increasingly employed to integrate environmental, morphological, and climatic variables into predictive surveillance systems[7].

Recent advances in drone-based remote sensing now allow centimetre-scale observation of urban environments, revealing relationships between built form, vegetation, and microclimate that govern *Aedes* habitat suitability[8–10]. Previous studies have suggested the application of remote sensing and aerial survey technologies for mosquito surveillance across tropical and subtropical regions[11]. Satellite-based analyses in Southeast Asia and Latin America have been used to map environmental suitability for *Aedes* mosquitoes by integrating land surface temperature, vegetation indices, and urban land-use patterns[12]. More recently, UAV-based approaches have enabled finer-scale detection of potential breeding habitats, including water-holding containers, vegetation clusters, and shaded micro-environments within residential areas[13]. In tropical urban settings with monsoon-driven climatic variability, seasonal fluctuations in rainfall, temperature, and vegetation growth have been shown to influence mosquito population dynamics and habitat persistence[14]. Remote sensing platforms, particularly UAVs, offer the capability to capture these temporal and spatial variations, supporting dynamic surveillance frameworks. However, most existing studies rely on coarse-resolution imagery or focus on macro-scale environmental predictors, with limited attention to microclimatic interactions such as vegetation–shade coupling at the neighbourhood scale[15,16].

However, most remote-sensing applications in dengue ecology still rely on coarse-resolution satellite imagery (e.g., MODIS, Sentinel-2) or city-level land-cover classes, which cannot resolve household-scale breeding environments such as drains, courtyards, and backyard vegetation[17,18]. In Malaysia, this limitation is particularly evident in mixed morphologies where terrace and high-rise housing coexist, generating diverse microclimatic and shading conditions that influence mosquito survival differently[19]. Paradoxically, urban greening initiatives intended to enhance heat-mitigation and climate resilience can also intensify dengue risk by expanding shaded, humid refugia near dwellings[20,21]. Addressing this paradox requires an analytical framework that explicitly links vegetation structure, shading intensity, and urban form within a computational modeling environment. Such integration aligns with the CEUS research agenda, which emphasizes data-driven urban analytics and environmental decision-support systems.

This study introduces a drone-based computational framework for mapping *Aedes*-prone microhabitats in Seksyen 24, Shah Alam, Selangor. High-resolution RGB orthomosaics were processed to derive vegetation (Excess Green Index, ExG) and shading (brightness) indices, combined into a Composite Ecological Risk Index (CERI) to quantify habitat suitability across contrasting morphologies[22–24]. The analysis integrates shade–vegetation interaction modeling, kernel-density hotspot detection, and directional shade analysis to capture micro-ecological variations that conventional surveys overlook[25].

Materials and methods

Study area

The study was conducted in Seksyen 24, Shah Alam, Selangor, Malaysia (3.02° N, 101.31° E) a dengue-endemic urban sector situated within the Klang River Basin (Fig. 1). The area experiences a tropical humid climate, with a mean annual temperature of approximately 27 °C and monthly rainfall exceeding 200 mm[26]. The study area was selected to capture a representative range of urban residential morphologies commonly found in Malaysian cities, including high-rise, medium-rise, and terrace housing types. Seksyen 24, Shah Alam, provides a heterogeneous urban landscape within a compact spatial extent, allowing controlled comparison of vegetation density, shading patterns, and built-form configurations across contrasting morphologies. This diversity makes the area a suitable testbed for examining micro-scale environmental drivers of *Aedes* habitat suitability. Four representative residential morphologies were selected to capture urban heterogeneity in built form, vegetation cover, and shading intensity. Site A (Flat B) represents a compact high-rise complex (8–12 floors) with low vegetation coverage (approx. 38%) and a high proportion of impervious surfaces (>70%). Site B (Flat H) comprises medium-rise residential blocks (4–6 floors) with moderate vegetation coverage (approx. 38%) and semi-enclosed shaded courtyards. Site C (Teres B) consists of dense terrace housing (1–2 floors) characterized by relatively low vegetation coverage (approx. 31%), high building density (approx. 60%), and narrow back-lane configurations. In contrast, Site D (Teres D) represents low-density terrace housing (1–2 floors) with higher vegetation coverage (approx. 50%), lower building density (approx. 45%), and more open spatial layouts with mature trees and grassed areas. Detailed quantitative characteristics of each morphology type are provided in Table 1. These contrasting morphologies reflect typical Malaysian urban typologies where differential shading and vegetation configurations influence *Aedes* habitat suitability. The four residential morphology types were classified based on a combination of building structure, spatial configuration, and vegetation characteristics derived from UAV orthomosaics and supported by cadastral data from the Shah Alam City Council (MBSA). Classification criteria included building height (high-rise vs. low-rise), housing density, spatial arrangement (clustered vs. linear), and the extent of surrounding vegetation. These features were visually and spatially distinguishable within the study area, allowing clear separation of morphology types with minimal overlap. The selected categories represent common residential typologies in Malaysian urban environments, facilitating comparative analysis of micro-environmental conditions across contrasting built forms. Site boundaries and coordinates were georeferenced to Shah Alam City Council cadastral data and verified against UAV orthomosaics for spatial accuracy.

UAV image acquisition and pre-processing

High-resolution imagery was acquired using a DJI Phantom 4 RTK UAV equipped with a 20-megapixel RGB camera (1-inch CMOS sensor, 8.8 mm focal length). A total of four UAV survey flights were conducted, with one flight per residential morphology site, to ensure consistent spatial coverage and minimize variability in environmental conditions. All flights were performed between 0900 h and 1100 h during clear-sky conditions to

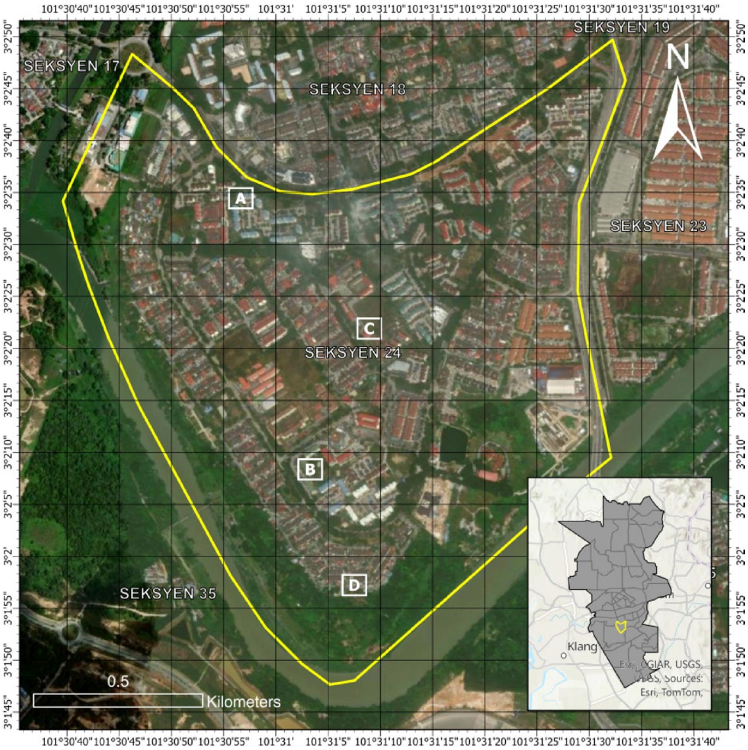

Fig. 1. Location of the study area in Seksyen 24, Shah Alam, Selangor, Malaysia. The study boundary is delineated on a UAV-derived orthophoto. All spatial data and maps were generated by the authors using UAV imagery processed in Agisoft Metashape Professional version 2.0 (https://www.agisoft.com/) and visualized using ArcGIS Pro version 3.1 (https://www.esri.com/) and QGIS version 3.34 (https://qgis.org/). No third-part y satellite imagery was used.

Parameter	Flat B (High-rise)	Flat H (Medium-rise)	Teres B (Dense terrace)	Teres D (Low-density terrace)
Building height (floors)	8–12	4–6	1–2	1–2
Building coverage (%)	~75	~65	~60	~45
Vegetation coverage (%)	~38	~38	~31	~50
Shaded vegetation (%)	12.6	9.4	6.7	11.9
Mean CERI	2.43 ± 0.38	2.08 ± 0.35	3.24 ± 0.51	3.87 ± 0.42
Spatial configuration	Compact cluster	Semi-clustered	Linear dense	Open + vegetated

Table 1. Quantitative characteristics of residential morphology types. Note: (~) approx.

reduce illumination variability and shadow distortion. All UAV operations were conducted over public spaces, and no personal or identifiable data were collected. Flights were performed during daylight under clear weather conditions, maintaining safe altitude and operational distances in accordance with the Manual of Aerodrome Standards (DCA Malaysia, 2022).

Flight missions followed a boustrophedonic (grid-based) pattern with 80% forward and 70% side overlap at an altitude of 80 m, resulting in a ground sampling distance (GSD) of approximately 2.5 cm per pixel. The total area covered by the orthomosaics across all sites was approximately 2.1 hectares, encompassing representative sections of each residential morphology. Images were processed in Agisoft Metashape Professional 2.0 (Agisoft LLC, St. Petersburg, Russia) to generate orthorectified mosaics and Digital Surface Models (DSMs), with radiometric normalization and geometric correction applied to ensure consistency and spatial accuracy. The final orthomosaics were exported as GeoTIFFs (EPSG: 4326 – WGS 84) for spatial analysis in ArcGIS Pro 3.1 (Esri, Redlands, CA, USA) and QGIS 3.34 (QGIS Development Team, Open Source Geospatial Foundation, USA). Georeferencing accuracy was evaluated based on the expected performance of the RTK-enabled UAV system and standard photogrammetric processing workflows. Previous studies report Root Mean Square (RMS) errors typically within the range of 0.03–0.10 m for RTK-based UAV mapping, which is considered sufficient for fine-scale spatial analysis in urban environments.

Computational workflow and spatial analysis

Orthomosaics were processed through a structured multi-step geospatial workflow integrating vegetation, shading, urban morphology, and ecological risk modelling (Table 2). All spatial analyses were conducted at the pixel level based on the UAV-derived ground sampling distance (GSD) of approximately 2.5 cm per pixel. Vegetation density was quantified using the Excess Green Index (ExG = 2G – R – B), a widely established RGB-based index for discriminating green vegetation in high-resolution imagery[22]. Vegetation density classes (dense, moderate, and low) were derived using a data-driven thresholding approach based on the distribution of ExG values. Histogram analysis was performed to identify natural breakpoints within the ExG range, and thresholds were subsequently defined to categorize vegetation into three classes. This approach ensures that classification reflects the underlying variability of vegetation intensity within the study area.

Shaded areas were delineated using brightness thresholding derived from RGB intensity values (threshold < 100), a commonly applied method for shadow detection in high-resolution remote sensing analyses[23]. The brightness threshold (< 100) was determined using histogram-based segmentation of RGB intensity values (0–255 scale), where a clear separation between shaded and non-shaded pixels was observed. This data-driven threshold is consistent with established approaches for shadow detection in high-resolution RGB imagery. Shaded zones were identified using brightness values derived from RGB imagery on an 8-bit scale ranging from 0 to 255, where lower values represent darker (shaded) areas. A threshold of < 100 was applied to delineate shaded regions based on histogram distribution.

Subsequent overlay analysis was performed to identify zones of shade–vegetation coupling, representing micro-environmental conditions conducive to *Aedes* habitat persistence. These coupled layers were normalized to a common scale and integrated using a weighted overlay approach to generate the Composite Ecological Risk Index (CERI). To ensure methodological transparency and reproducibility, all environmental variables were standardized prior to integration into the Composite Ecological Risk Index (CERI) using a min–max normalization approach. Continuous raster layers for vegetation (ExG) and shading (brightness) were rescaled to a common range (0–1) using the following transformation:

$$X_{\mathrm{norm}} = \frac{X - X_{\min}}{X_{\max} - X_{\min}}$$

where X represents the original pixel value, and X_{min} and X_{max} correspond to the minimum and maximum values of the respective raster layer.

The shading component was derived from RGB brightness values (0–255 scale), where lower values represent darker (shaded) areas. Initially, a threshold of < 100 was used to delineate shaded zones for spatial overlay analysis. For integration into the CERI model, brightness values were retained as a continuous variable and subsequently normalized using the min–max transformation. To enhance interpretability, the normalized shading layer was inverted such that higher values represent greater shading intensity:

$$\mathrm{Shade}_{\mathrm{norm}} = 1 - \frac{\mathrm{Brightness} - \mathrm{Brightness}_{\min}}{\mathrm{Brightness}_{\max} - \mathrm{Brightness}_{\min}}$$

The Composite Ecological Risk Index (CERI) was then computed using an equal-weighted linear combination of normalized vegetation and shading layers:

$$\mathrm{CERI} = 0.5 \times \mathrm{ExG}_{\mathrm{norm}} + 0.5 \times \mathrm{Shade}_{\mathrm{norm}}$$

The resulting CERI values were rescaled to a 0–5 range for interpretability and subsequently classified into three ecological risk categories: low (0–2), moderate (2–3), and high (≥ 3). The threshold of CERI ≥ 3 was used to

Step	Objective/Parameter	Method/Formula	Software/Tool	Output/Application
Vegetation Index (ExG)	Quantify vegetation density and green cover	ExG = 2G – R – B (normalized RGB reflectance)	ArcGIS Pro 3.1/QGIS 3.34	Classified vegetation map (dense > 30; moderate 10–30; low < 10); % vegetation per morphology
Shade Detection	Identify shaded zones from brightness layer	Histogram segmentation, threshold < 100 (mean brightness)	ArcGIS Pro 3.1/Raster Calculator	Binary shade raster showing canopy/building shadows
Shade–Vegetation Coupling	Map overlap between vegetation and shaded pixels	Raster overlay (ExG > 30 ∩ Brightness < 100)	ArcGIS Pro 3.1	Shaded-vegetation coupling zones (m^2, %) per site
Composite Ecological Risk Index (CERI)	Integrate vegetation and shading into a continuous risk model	Weighted overlay (equal weight; 0–5 scale via min–max normalization)	ArcGIS Pro 3.1	Composite risk map (0–5 scale) classified into three categories: low (0–2), moderate (2–3), and high (≥ 3)
Morphological Correlation	Relate built-form density to vegetation and risk	Digitized building footprint (%), Pearson correlation ($p < 0.05$)	QGIS 3.34/IBM SPSS 29	Correlation matrix (building coverage vs. vegetation & risk)
Spatial Hotspot Detection (KDE)	Identify spatial clusters of ecological risk	Kernel Density Estimation; 15 m search radius, quartic kernel	ArcGIS Pro 3.1	Hotspot heatmap using a yellow–red gradient to represent increasing risk levels (yellow = low risk; red = high risk)
Directional Shade Gradient Analysis	Examine orientation-driven shade persistence	Solar azimuth & façade direction via DSM; 8 cardinal classes	QGIS 3.34 Solar Radiation Plugin	Rose diagrams of shade persistence (%) and vegetation adjacency (≤ 5 m)

Table 2. Summary of computational workflow for *Aedes* habitat-risk modeling.

define high-risk areas for subsequent statistical and spatial analyses. The CERI was developed in this study as an integrative spatial metric that combines vegetation density and shading intensity, following established principles of spatial multi-criteria risk modelling[24]. This approach enables the transformation of discrete environmental variables into a unified ecological risk surface, facilitating fine-scale identification of *Aedes*-prone microhabitats within heterogeneous urban landscapes. Spatial correlation between building density and vegetation–shade variables was analyzed using Pearson coefficients ($p < 0.05$). Kernel Density Estimation (KDE) identified hotspot clusters of ecological risk, and Directional Shade Gradient Analysis derived from DSM-based solar azimuth quantified orientation-dependent shade persistence. Kernel Density Estimation (KDE) was applied to the spatial distribution of CERI values to identify clusters of ecological risk. KDE was performed using a quartic kernel with a fixed bandwidth (search radius) of 15 m. This bandwidth was selected based on the spatial scale of residential features and typical dispersal distances of *Aedes* mosquitoes. Sensitivity testing using alternative bandwidths (10–20 m) yielded consistent hotspot patterns, supporting the robustness of the selected parameter. Specifically, KDE was computed using pixels classified as moderate-to-high risk (CERI ≥ 3), enabling detection of spatial *Aedes*-prone microhabitats. The complete stepwise analytical workflow from UAV-derived orthomosaics to final CERI classification is summarized in Fig. 2.

Data analysis

The analytical workflow transformed UAV-derived imagery into quantifiable ecological indicators of *Aedes* habitat suitability. Orthomosaics were processed to extract vegetation (ExG) and brightness indices, which were then combined to delineate shaded-vegetation overlaps microhabitats conducive to mosquito survival. These parameters were normalized into CERI risk scores and classified into low, moderate, and high categories. Spatial clustering (KDE) and orientation analysis quantified micro-scale patterns of habitat persistence. Statistical validation tested the association between built-form density, vegetation coverage, and ecological risk, enabling fine-scale ecological mapping for a promising complementary tool for precision surveillance. To assess differences in vegetation density, shaded–vegetation coupling, and CERI across residential morphology types, statistical comparisons were performed using the Kruskal–Wallis test due to non-normal distribution of the data. Where significant differences were detected, post hoc pairwise comparisons were conducted using Dunn's test with Bonferroni correction. Statistical significance was set at $p < 0.001$. Building coverage was calculated as the proportion of built-up surface area derived from UAV orthomosaics, representing the extent of impervious surfaces within each study site. This metric is conceptually comparable to sealing layer indicators used in urban land-use datasets.

To evaluate whether vegetation–shade coupling exerted a synergistic effect, two hierarchical models were developed using pixel-level CERI values as the dependent variable. The beta regression model was specified as: logit(CERI) = $\beta_0 + \beta_1$(Vegetation) + β_2(Shade) + β_3(Vegetation × Shade) The logistic regression model for high-risk classification (CERI ≥ 3) was defined as: logit(P(high-risk)) = $\beta_0 + \beta_1$(Vegetation) + β_2(Shade) +

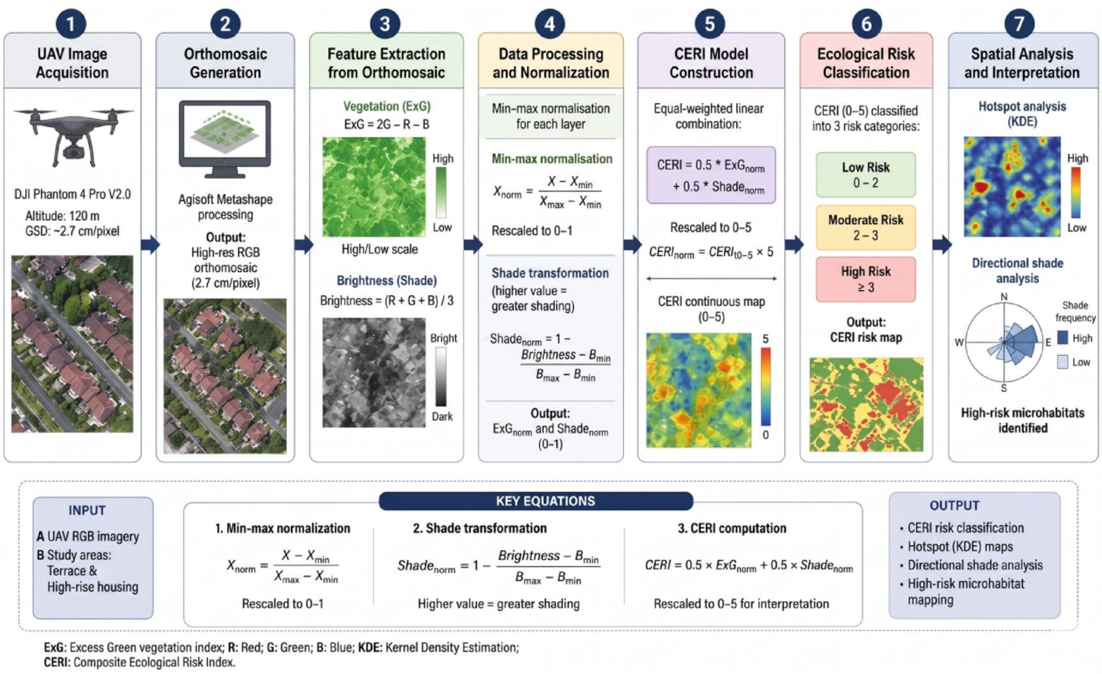

Fig. 2. Stepwise computational workflow for deriving the Composite Ecological Risk Index (CERI) from UAV-derived RGB orthomosaics. The pipeline illustrates sequential processing from image acquisition and feature extraction (vegetation and shading indices) to normalization, model integration, ecological risk classification, and spatial analysis.

β_3(Vegetation × Shade). The additive model (M_0) included vegetation and shading as independent predictors, whereas the interaction model (M_1) incorporated their multiplicative term (Vegetation × Shade) to capture potential synergistic effects. Model performance was assessed using both beta regression for continuous CERI values and logistic regression for high-risk classification (CERI ≥ 3). Predictor variables were standardized prior to analysis, and multicollinearity was evaluated using the variance inflation factor (VIF < 3). Comparative model performance was evaluated using Akaike Information Criterion (AIC), Bayesian Information Criterion (BIC), pseudo-R^2, and 10-fold cross-validation root mean square error (RMSE). Likelihood Ratio Tests (LRT) were used to assess the significance of the interaction term, with $\Delta AIC > 10$ and $p < 0.05$ indicating substantial model improvement. Residual spatial autocorrelation was examined using Moran's I to ensure independence of model residuals following spatial smoothing. All statistical analyses were conducted using IBM SPSS Statistics 29 (IBM Corp., Armonk, NY, USA).

Results

Vegetation density and potential *Aedes* resting habitats

Analysis of the UAV-derived RGB orthomosaics using the Excess Green (ExG) index revealed distinct spatial heterogeneity in vegetation density across the four residential morphologies in Seksyen 24, Shah Alam (Fig. 3). Terrace housing (*Teres D*) recorded the highest dense vegetation coverage (approx. 50%), followed by *Flat H* and *Flat B* (approx. 38%), while *Teres B* exhibited the lowest (approx.31%). Vegetation cover was higher in terrace areas compared to high-rise morphologies, and these differences were statistically significant (Kruskal–Wallis test, $p < 0.001$). Quantitative differences between morphology types are summarized in Table 1, highlighting clear variation in building density, vegetation coverage, and ecological risk. Dense vegetative structures were identified as areas with higher vegetation index values, corresponding to increased spatial coverage of vegetated zones across the study sites.

Shade–vegetation coupling and microhabitat suitability

Overlay analysis of shaded areas (brightness < 100) and densely vegetated areas (ExG > 30) identified distinct shade–vegetation coupling zones indicative of high *Aedes* microhabitat potential (Fig. 4A–B). The extent of shaded–vegetation coupling varied across residential morphologies: Flat B exhibited the largest coverage (421.3 m^2; 12.6%), followed by Teres D (398.7 m^2; 11.9%), Flat H (315.2 m^2; 9.4%), and Teres B (218.4 m^2; 6.7%). The extent of shaded–vegetation coupling differed significantly across residential morphologies (Kruskal–Wallis $H = 18.72$, $df = 3$, $p < 0.001$), suggesting heterogeneity in the spatial distribution of coupled vegetation–shade zones. Overall, higher shaded–vegetation proportions observed in Flat B and Teres D suggested areas of greater overlap between vegetation and shading within the study sites.

Composite ecological risk and habitat suitability

The Composite Ecological Risk Index (CERI), integrating ExG and brightness layers, produced continuous risk surfaces (0–5 scale) illustrating spatial differentiation in *Aedes* habitat suitability (Fig. 5A–B). The mean CERI scores ranked as follows: *Teres D* = 3.87 ± 0.42; *Teres B* = 3.24 ± 0.51; *Flat B* = 2.43 ± 0.38; *Flat H* = 2.08 ± 0.35. High-risk zones (≥ 3) accounted for 46.5% of *Teres D*, 41.2% of *Teres B*, 13.4% of *Flat B*, and 11.5% of *Flat H*. The CERI values differed significantly across residential morphologies (Kruskal–Wallis $H = 21.36$, $df = 3$, $p < 0.001$), indicating variation in ecological risk levels among study sites. Spatially, terrace morphologies displayed risk concentrations along backyard corridors, vegetated compounds, and canopy-overlap areas features absent

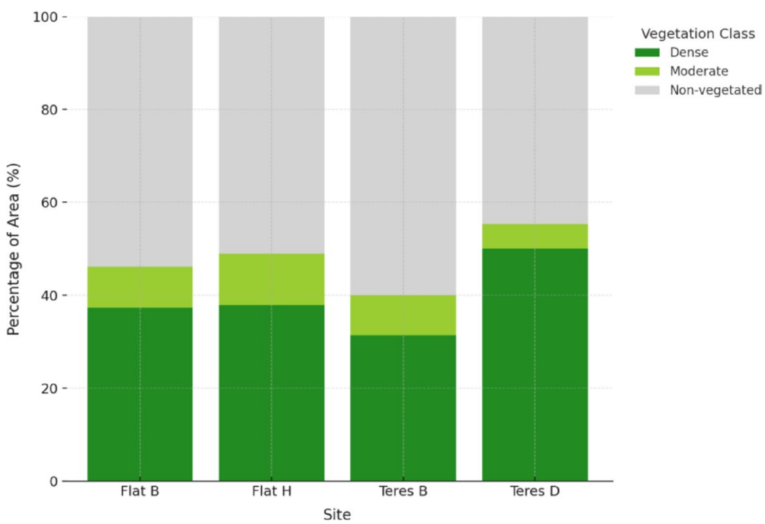

Fig. 3. Spatial distribution of vegetation density derived from the UAV-derived RGB orthomosaics. Vegetation was classified using the Excess Green Index (ExG) into three categories: dense (> 30), moderate (10–30), and low (< 10). The bar chart illustrates the proportion of vegetation classes across the four residential morphologies.

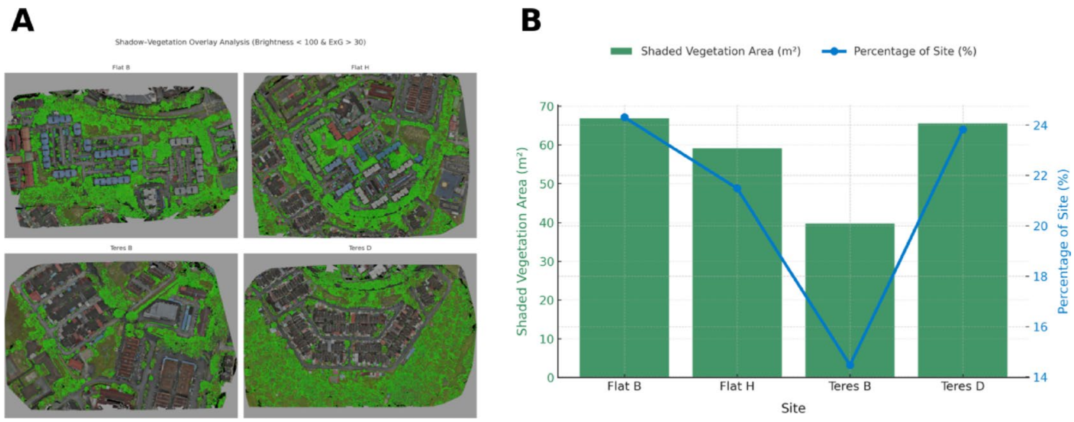

Fig. 4. Spatial distribution and quantification of shade–vegetation coupling across residential morphologies. **(A)** Overlay analysis derived from the integration of vegetation (Excess Green Index, ExG) and brightness-based shading layers (brightness < 100), where green-highlighted areas represent zones of shade–vegetation coupling. **(B)** Bar chart showing shaded vegetation area (m^2) and corresponding percentage of site coverage across the four residential morphologies. All spatial layers were derived from UAV orthomosaics processed in Agisoft Metashape Professional version 2.0 and analyzed using ArcGIS Pro version 3.1. Figures were prepared by the authors without use of external satellite imagery.

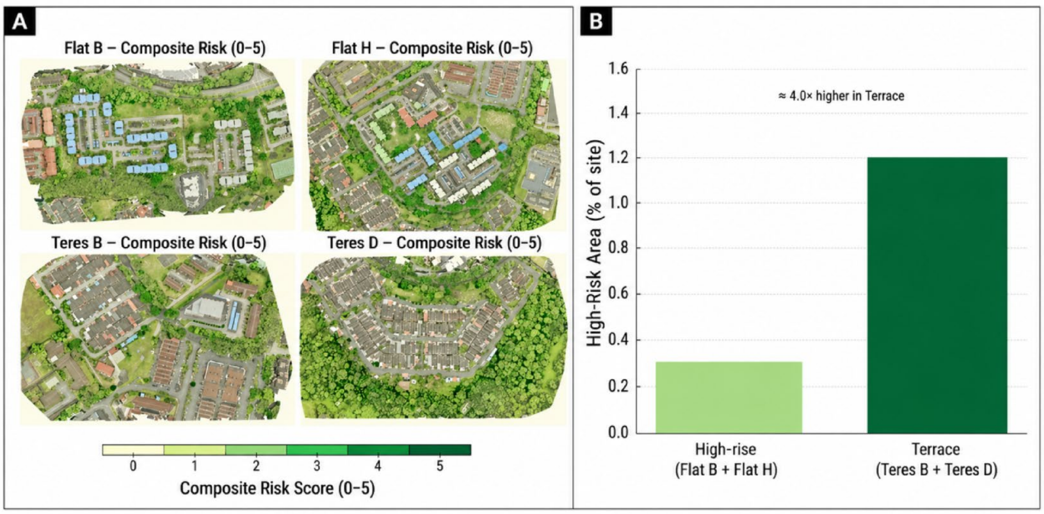

Fig. 5. **(A)** Spatial distribution of composite risk (0–5) integrating vegetation and shading layers. **(B)** Comparison of morphology types showing terrace environments exhibiting approx. 4× greater high-risk coverage than high-rise complexes. Spatial analysis and visualization were conducted using ArcGIS Pro version 3.1 and QGIS version 3.34. All imagery was generated from UAV data processed by the authors.

in compact high-rise typologies. Composite risk values above 3.0 suggested humid, shaded microhabitats highly conducive to *Aedes* persistence, while scores below 2.0 represent thermally exposed, low-vegetation environments.

To ensure appropriate ecological interpretation, high CERI values should be understood as indicators of environmental suitability for *Aedes* persistence, rather than direct evidence of mosquito presence or potential breeding habitats. Specifically, areas with elevated CERI scores reflect micro-environmental conditions characterized by dense vegetation and persistent shading, which are known to support adult mosquito resting behaviour, reduce desiccation risk, and create favourable conditions for oviposition and larval survival. Thus, the identified high-risk zones represent *Aedes*-prone microhabitats encompassing both potential resting environments and suitable ecological conditions for breeding, rather than discrete or verified larval habitats.

Across all residential morphologies, descriptive statistics suggested substantial variability in environmental indices within the study area. The Composite Ecological Risk Index (CERI) had an overall mean of 2.91 ± 0.78, with values ranging from 1.12 to 4.76. Vegetation (ExG) values exhibited moderate variability (mean = 28.4 ± 9.6, range = 10.2–52.7), while brightness-based shading values showed a wider distribution (mean = 112.6 ± 24.3,

Variable	Mean ± SD	Median (IQR)	Min	Max
ExG (Vegetation Index)	28.4 ± 9.6	27.9 (21.3–34.8)	10.2	52.7
Brightness (Shade Index)	112.6 ± 24.3	109.5 (95.2–128.7)	68.5	168.9
CERI	2.91 ± 0.78	2.85 (2.21–3.54)	1.12	4.76
Shaded–Vegetation (%)	10.2 ± 3.1	9.8 (7.4–12.9)	4.8	16.7

Table 3. Descriptive statistics of ecological indices across all residential morphologies.

Variable	Statistic (H)	*p*-value	Post hoc (Dunn–Bonferroni)	Interpretation
Vegetation Density (ExG)	18.72	< 0.001	Teres D > Flat H, Flat B; Teres B > Flat B	Significant differences across morphologies
Shaded–Vegetation Area (%)	15.43	< 0.001	Flat B > Teres B; Teres D > Flat H	Significant variation in coupling zones
CERI (0–5)	22.91	< 0.001	Teres D > Flat H, Flat B; Teres B > Flat H	Terrace areas significantly higher risk
High-Risk Proportion (CERI ≥ 3)	20.36	< 0.001	Teres D > all; Teres B > Flat B, Flat H	Strong morphology-driven risk pattern

Table 4. Statistical comparison of ecological indicators across residential morphology types. Note: Statistical comparison of ecological indicators across residential morphology types using Kruskal–Wallis test and Dunn's post hoc analysis with Bonferroni correction. Significant differences were observed across all variables ($p < 0.001$).

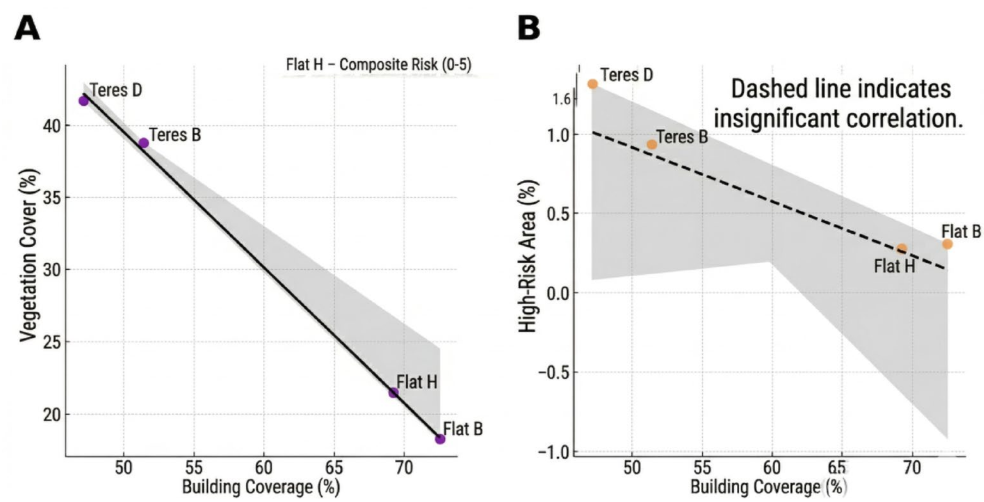

Fig. 6. Correlations between building density, vegetation cover, and ecological risk. **(A)** Strong negative correlation ($r = -0.97$, $p = 0.03$) between building coverage and vegetation. **(B)** Moderate negative relationship ($r = -0.83$, $p = 0.17$) between building coverage and high-risk area.

range = 68.5–168.9). The proportion of shaded–vegetation coupling areas averaged 10.2 ± 3.1%, ranging from 4.8% to 16.7% across all sites. These results reflect the heterogeneous micro-environmental conditions across residential morphologies. Detailed summary statistics are provided in Table 3.

To statistically validate these observed differences, non-parametric comparisons were performed across residential morphology types. The Kruskal–Wallis test revealed significant differences in vegetation density, shaded–vegetation coupling, and CERI values across all sites ($p < 0.001$). Post hoc Dunn's tests with Bonferroni correction suggesting that terrace morphologies (Teres D and Teres B) exhibited significantly higher ecological risk compared to high-rise forms (Flat B and Flat H). These findings provide statistical support for the spatial patterns observed in the composite risk maps (Table 4).

Morphological determinants of ecological risk

Correlation analysis (Fig. 6) suggesting that built-form density strongly regulates ecological vulnerability. Building coverage was negatively correlated with vegetation cover ($r = -0.97$, $p = 0.03$). However, it was not significantly correlated with high-risk areas ($r = -0.83$, $p = 0.17$). Thus, compact morphologies suppress vegetation availability, while open layouts such as terrace housing increase exposure to ecological risk. These results suggested that higher building coverage is associated with reduced vegetation availability. However, its relationship with high-risk ecological areas was not statistically significant, suggesting that additional environmental factors may influence spatial risk patterns. These findings support the hypothesis that urban porosity and green connectivity amplify vector-suitable microhabitats.

Statistical evidence for vegetation–shade interaction

Inclusion of the Vegetation × Shade interaction term substantially improved model performance relative to additive forms (Table 5). For the continuous CERI model, pseudo-R^2 increased from 0.41 to 0.56 ($\Delta R^2 = +0.15$), while AIC decreased by 35.2 units (612.8 → 577.6). The observed increase in pseudo-R^2 (+0.15) and reduction in AIC (>35 units) represent substantial improvements in model explanatory power, indicating a strong effect size associated with vegetation–shade interaction. Likelihood Ratio Testing confirmed the superiority of the interaction model ($\chi^2 = 28.9$, df = 1, $p < 0.001$). Cross-validation error declined by 14%, confirming predictive robustness. The logistic model for high-risk pixels (CERI ≥ 3) yielded McFadden $R^2 = 0.39$ (vs. 0.27 additive), with AIC/BIC reductions of 31.4 and 25.6. The interaction coefficient ($\beta = 0.63 \pm 0.11$, $p < 0.001$) suggested that risk increased disproportionately when both vegetation and shading were high, with predicted probabilities rising from 32% to 68%. The interaction coefficient ($\beta = 0.63 \pm 0.11$, $p < 0.001$; 95% CI: 0.41–0.85) suggests a positive synergistic effect between vegetation and shading on ecological risk. Predicted probabilities of high-risk conditions increased from 32% (95% CI: 28–36%) to 68% (95% CI: 62–73%) under combined high vegetation and shading conditions. These metrics empirically validate that vegetation–shade synergy explains *Aedes* microhabitats more effectively than independent predictors.

Spatial hotspot detection of *Aedes*-prone micro-environments

Kernel Density Estimation (KDE) of composite risk values revealed statistically significant clusters of ecological risk across all morphologies (Fig. 7A–D). The most intense *Aedes*-prone microhabitats occurred along interfaces between shaded vegetation and built-up structures zones typically associated with container accumulation and roof drains. *Teres D* and *Flat B* exhibited the highest hotspot intensities among the studied morphologies.

Directional shade gradient and orientation-driven persistence

Directional Shade Gradient Analysis (Fig. 8) showed that microclimatic conditions conducive to *Aedes* persistence are orientation-dependent. North- and east-facing façades exhibited the highest shade persistence and vegetation adjacency (ExG > 30 within 5 m), receiving limited solar exposure during peak hours. Terrace morphologies displayed the strongest directional effects, indicating that façade orientation and geometry shape micro-scale thermal refugia that extend mosquito survival and larval development.

Morphological pattern classification and ground validation

Ground validation through field inspection and visual comparison with UAV-derived orthomosaics confirmed four principal morphological typologies that consistently aligned with model-identified high-risk zones (Supplementary Table S6). The Building Perimeter Patterns, encompassing north- and east-facing façades and corridor edges, exhibited persistent shading throughout the day, providing ideal sheltered resting environments for adult *Aedes* mosquitoes. Architectural Interface Patterns, typically located at building corners and junctions, created semi-enclosed microclimates with restricted air circulation and elevated surface moisture, further enhancing mosquito refuge potential. Organized Vegetation Patterns, represented by linear rows of shade trees in parking areas, produced continuous canopy cover and maintained cooler, more humid soil surfaces conducive to larval and adult survival. Meanwhile, Private Realm Patterns, including rear-yard vegetation clusters and boundary hedges, exhibited the longest shade duration and strongest vegetation–shade coupling, often in poorly maintained or secluded domestic spaces. Collectively, these morphological configurations substantiate the spatial models, demonstrating that micro-scale architectural and vegetative arrangements directly influence the persistence of shade and humidity. The strong correspondence between drone-based analytical outputs and ground observations reinforces the conclusion that fine-grained urban design particularly façade orientation, vegetation organization, and enclosure geometry plays a critical role in governing *Aedes* habitat suitability, persistence, and ecological resilience within urban residential landscapes.

Discussion

This study provides new spatial and computational evidence that vegetation density, shading intensity, and built-form geometry interact to shape the micro-ecological framework of *Aedes* mosquito habitats in tropical urban landscapes. The framework is designed as a proxy-based environmental risk assessment, capturing micro-environmental conditions associated with *Aedes* habitat suitability rather than directly measuring mosquito presence. These findings suggest that areas characterized by high vegetation density and persistent shading may

Model Type	Metric	Additive (M_0)	Interaction (M_1)	Improvement
Beta (CERI)	Pseudo-R^2	0.41	**0.56**	+ 0.15
	AIC	612.8	**577.6**	−35.2
	CV-RMSE	0.284	**0.244**	−14%
Logistic (CERI ≥ 3)	McFadden R^2	0.27	**0.39**	+ 0.12
	AIC/BIC	484.3/492.8	**452.9/467.2**	−31.4/− 25.6

Table 5. Comparison of additive (M_0) and interaction (M_1) models demonstrating improved fit with the Vegetation × Shade term. Note: All predictors standardized; VIF < 3; Moran's I ns after spatial smooth.

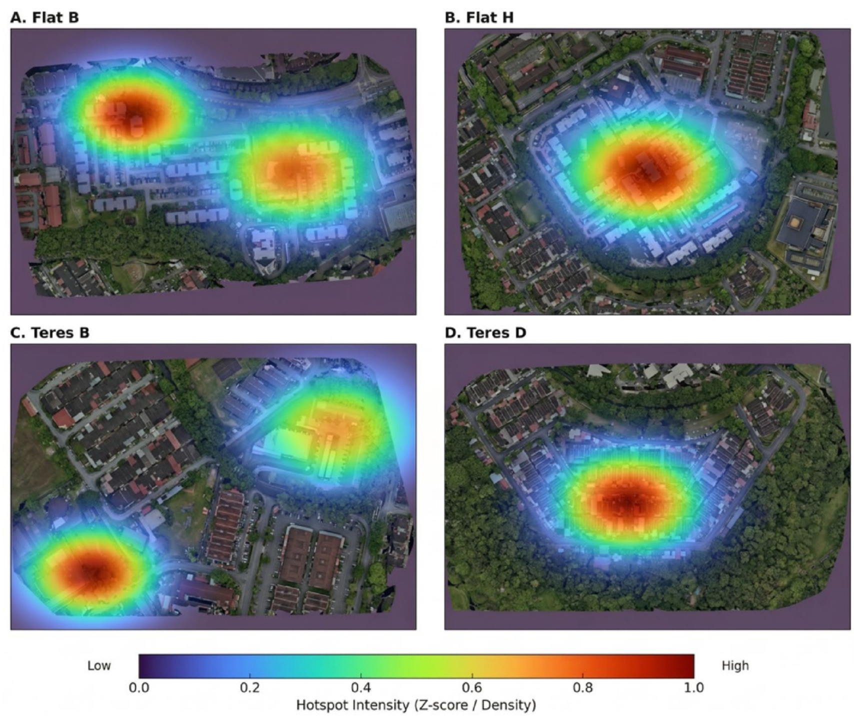

Fig. 7. Spatial distribution of *Aedes*-prone hotspot intensity derived from KDE analysis across residential morphologies. Panels **(A–D)** represent different study sites. Color gradients from dark-blue–cyan suggest low values for *Aedes* hotspot intensity, transitioning to warmer colors (yellow–red) indicating higher hotspot intensity. Spatial analyses were performed using ArcGIS Pro version 3.1. The base spatial layers were derived from UAV orthomosaics generated by the authors.

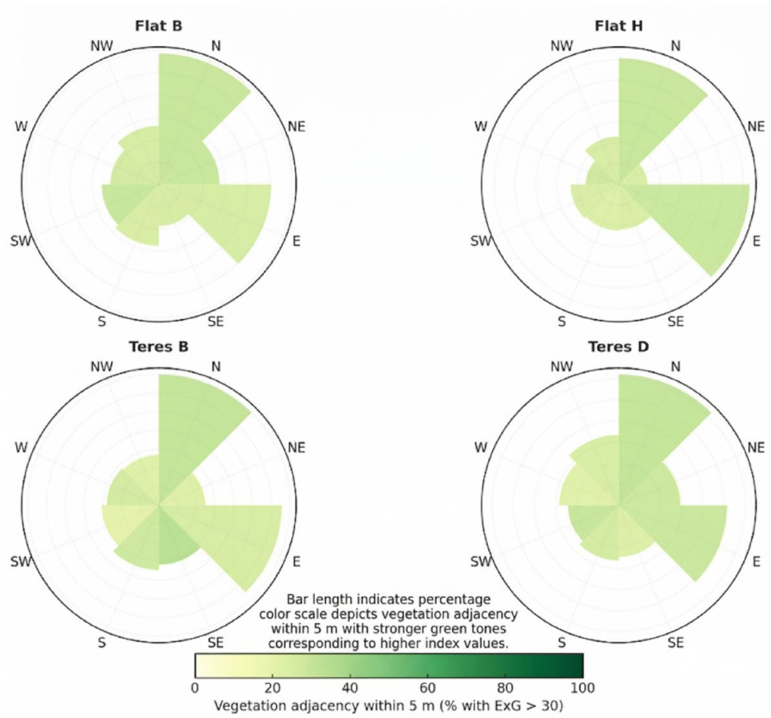

Fig. 8. Directional Shade Gradient Analysis showing orientation-driven shade–vegetation interactions across morphologies. Bar length = percentage of shaded façade; color = vegetation adjacency within 5 m (ExG > 30). North- and east-facing façades maintain prolonged shading.

create favorable microclimatic conditions, including reduced temperature and increased humidity, which have been associated with *Aedes* resting and oviposition behaviour. Through high-resolution UAV orthomosaics, we suggested that terrace morphologies with greater vegetation density and lower building coverage exhibited markedly higher ecological risk compared with compact high-rise complexes. These findings reveal a persistent paradox in tropical urban design: while urban greening mitigates heat stress, it simultaneously generates shaded and humid micro-habitats that favour *Aedes* persistence. Dense vegetation and sustained shading enhance adult resting sites, prevent larval desiccation, and maintain high relative humidity microclimatic conditions repeatedly associated with dengue transmission across Southeast Asia[27–30].

Importantly, the CERI framework should be interpreted as a proxy-based environmental suitability model, rather than a direct measure of *Aedes* population density or breeding site confirmation. The index integrates vegetation density and shading intensity to identify micro-environmental conditions that are ecologically favourable for mosquito persistence. High CERI values therefore represent general environmental suitability, encompassing both potential adult resting habitats and conditions conducive to oviposition and larval development, rather than explicitly delineating active potential breeding habitats. This distinction is particularly important in the absence of direct entomological validation and underscores the role of CERI as a complementary spatial decision-support tool for identifying priority areas for targeted surveillance and intervention.

The identification of shaded-vegetation overlap zones (brightness < 100; ExG > 30) as high-risk habitats aligns with spatial entomology research showing that vegetation continuity and shade persistence explain fine-scale variability in *Aedes aegypti* abundance[31,32]. By quantifying shaded vegetation area from 218 m² in *Teres B* to 421 m² in *Flat B* and linking these directly to composite ecological risk, this study advances current understanding by translating micro-environmental conditions into measurable spatial indicators. The coupling of vegetation and shade forms localized thermal refugia that moderate surface temperature and extend larval viability factors that can now be detected, quantified, and mapped automatically using UAV analytics. This represents a methodological leap from descriptive ecology to computational environmental modeling, enabling systematic surveillance at scales previously inaccessible through field observation[33]. The Composite Ecological Risk Index (CERI) revealed that terrace housing contained almost four times more high-risk area (score ≥ 3) than high-rise morphologies, suggesting that open layouts and backyard vegetation intensify habitat suitability. These findings suggest that horizontal density and vegetation persistence may play a more influential role than building height in shaping ecological vulnerability across urban residential morphologies. These patterns mirror findings from Singapore, Bangkok, and Jakarta, where suburban terrace developments remain dengue-prone despite lower population densities[34–36]. By deriving these risk surfaces from aerial imagery, this study suggests how drone-based sensing has the potential to augment, rather than replace, conventional surveillance methods with automated, predictive mapping of *Aedes*-prone microhabitats. Kernel-density mapping further localized statistically significant clusters along built–vegetation interfaces precisely the micro-zones where gutters, drains, and discarded containers accumulate. Such evidence supports a transition from blanket fogging toward a promising complementary tool for precision surveillance, where interventions target ecologically validated risk clusters instead of administrative boundaries. A particularly novel contribution of this work is the detection of orientation-dependent shade persistence. Directional analysis showed that north- and east-facing façades sustained the longest shade durations and greatest vegetation adjacency (ExG > 30 within 5 m). These façades, receiving less direct afternoon sunlight, maintain cooler, more humid conditions conducive to *Aedes* oviposition. The integration of solar geometry with ecological metrics extends drone analytics into the third dimension linking façade orientation and vertical form to habitat persistence. Such data enable 3D risk visualization, allowing local authorities to identify not just surface *Aedes*-prone microhabitats but also vulnerable building orientations. When integrated into municipal dashboards, this capability could inform inspection priorities, community clean-ups, and façade-specific environmental design guidelines.

These observed differences likely reflect variation in canopy maturity, vegetation density, and building configuration across residential morphologies. High-rise environments such as Flat B, despite limited ground-level vegetation, can generate extensive shaded areas through overlapping building shadows on courtyard greenery. In contrast, compact terrace forms such as Teres B may limit both sunlight interception and vegetation development, reducing the extent of shade–vegetation coupling. Areas characterized by dense vegetation (ExG > 30) and persistent shading (brightness < 100) may create localized micro-environmental conditions, including reduced temperature and increased humidity, which have been associated with *Aedes* resting and oviposition behaviour. The higher shaded–vegetation overlap observed in *Flat B* and *Teres D* therefore suggests the presence of more persistent microclimatic conditions that may support mosquito survival.

Formal statistical comparison between additive and interaction models suggesting that vegetation–shade coupling is the one of the key environmental drivers of *Aedes*-prone microhabitat suitability. Including the Vegetation × Shade term improved pseudo-R^2 from 0.41 to 0.56 and reduced AIC by > 35 units, indicating a substantially better model fit. Sensitivity analyses, including variation in KDE bandwidth (10–20 m) and alternative model specifications, produced consistent spatial patterns and model performance, supporting the robustness of the findings. This synergy underscores that the coexistence of dense vegetation and persistent shading amplifies ecological risk far beyond additive effects a finding consistent with the "synergistic habitat" hypothesis proposed in tropical entomological modelling[27]. The strong performance of the interaction model validates the conceptual framework underlying the CERI, highlighting the advantage of integrated spatial indices over single-factor predictors for urban health analytics.

Collectively, these results establish drone-based ecological surveillance as a transformative decision-support tool for vector control. Conventional surveillance manual larval surveys and ovitrap inspections is reactive, costly, and spatially constrained[37–39]. In contrast, UAV orthomosaics can capture large residential sectors, extract vegetation and shading indices, and generate composite risk layers within hours. This supports the creation of Dynamic *Aedes* Risk Maps (DARM) automated, continuously updated layers that health authorities can integrate with epidemiological databases[40,41]. Such integration aligns with the World Health Organization's Integrated Vector Management (IVM) principles, which prioritize environmental modification and data-driven decision-making over routine chemical control[42]. Furthermore, UAV surveillance reduces occupational exposure, lowers inspection costs, and ensures coverage of otherwise inaccessible zones such as high-density flats, riverbanks, or informal settlements[43].

From a policy perspective, institutionalizing UAV monitoring could enable local councils to implement predictive environmental management rather than reactive outbreak response[44]. Regular drone flights can track vegetation growth, detect new shade accumulation, and assess compliance with sanitation bylaws[45]. When complemented by community engagement, visual evidence from drone imagery can enhance public understanding of how household vegetation and waste practices influence dengue risk[46]. Such participatory visualization fosters accountability and behavioral change, transforming drones from surveillance instruments into communication tools that support co-produced urban health governance[47]. These findings should be interpreted within the context of model-based inference, where uncertainty and variability are inherent. This study is based on environmental and spatial modelling of *Aedes*-prone microhabitats and does not include direct entomological validation such as larval indices, ovitrap data, or adult mosquito counts. Therefore, the results should be interpreted as indicators of ecological suitability rather than suggesting vector presence. Future studies should integrate UAV-derived environmental metrics with field-based entomological data to validate and enhance predictive accuracy.

Despite these advances, several limitations must be acknowledged. While the study area encompasses diverse residential typologies, it represents a single urban locality and may not fully capture the variability present across different cities or climatic regions. Therefore, the findings should be interpreted as context-specific. Future studies should extend this framework to multiple urban settings to evaluate its generalizability and robustness under varying environmental and morphological conditions. First, this study inferred ecological risk solely from environmental proxies without concurrent entomological validation (e.g., larval or adult density). Future work should pair UAV-derived indices with field sampling to calibrate risk thresholds; for instance, correlating CERI ≥ 3 with an ovitrap index $> 10\%$. Second, the analysis was cross-sectional, capturing a single temporal snapshot; seasonal drone surveys could reveal how vegetation phenology and solar trajectories alter habitat persistence across wet and dry seasons. Third, the study focused on one urban section of Shah Alam; applying the framework to multiple districts would strengthen generalizability and facilitate regional risk benchmarking. Lastly, although RGB imagery is cost-efficient, it cannot measure surface temperature or moisture directly.

Conclusion

In conclusion, this study suggested the potential of drone-enabled spatial analytics to enhance how urban environments are monitored, modelled, and managed in dengue-endemic settings. Terrace neighborhoods characterized by dense and persistent shaded vegetation were identified as the most ecologically vulnerable, whereas high-rise complexes exhibited more localized risk concentrated at built–vegetation interfaces. These findings highlight the critical role of vegetation–shade interactions and urban morphology in shaping fine-scale *Aedes* habitat suitability. By integrating high-resolution orthomosaic imagery with computational indices of vegetation and shading, the proposed framework provides a replicable and data-rich approach for identifying micro-scale ecological risk. This enables more precise, spatially targeted interventions compared to conventional surveillance methods. The ability to quantify and map these interactions further supports the development of Dynamic *Aedes* Risk Mapping (DARM), translating environmental data into actionable intelligence for vector control.From a practical perspective, incorporating UAV-based analytics into dengue prevention strategies could support early risk detection, prioritization of high-risk zones, and more informed urban planning decisions. Ultimately, this approach offers a pathway toward climate-sensitive, data-driven, and vector-smart urban systems that balance green infrastructure development with public health resilience.

Data availability

The datasets generated and analyzed in this study are not publicly available due to privacy and geolocation restrictions associated with drone-captured imagery in residential areas. Processed orthomosaic layers, vegetation (ExG) indices, and composite ecological risk maps can, however, be shared by the corresponding author upon reasonable request for research or educational purposes, subject to approval by the Universiti Teknologi MARA Research Ethics Committee (REC/FSK/2025/001). Derived analytical codes and model scripts used for vegetation–shade coupling, kernel density estimation, and composite ecological risk index (CERI) computation were developed in ArcGIS Pro 3.1, QGIS 3.34, and IBM SPSS v29, and are available from the authors on request to facilitate replication and further methodological development. All data were stored within UiTM's secure institutional repository and managed under the Research Data Management Policy (UiTM-RMC, 2024), ensuring compliance with national data-protection and research-integrity standards.

Received: 24 December 2025; Accepted: 6 May 2026
Published online: 14 May 2026

References

1. Enitan, S. S. et al. Advancing dengue fever preparedness in Africa: Challenges, resilience, and contributions to global health. *Acta Elit Salutis* **9** (1), 1–22 (2024).
2. Khan, A. et al. Vector-borne disease and climate change. In Arthropods—New Advances and Perspectives. IntechOpen. (2023).
3. Alipitchay, S. et al. Temporal and interaction dynamics of dengue cases, entomological and meteorological variables in Melaka, Malaysia: A multivariate time series analysis. *PLoS One* **20**(4), e0321273 (2025).

4. Ahmad Zaki, Z., Che Dom, N. & Ahmed Alhothily, I. Efficacy of *Bacillus thuringiensis* treatment on *Aedes* population using different applications at high-rise buildings. *Trop. Med. Infect. Dis.* **5**(2), 67 (2020).
5. Liu, Q. M., Gong, Z. Y. & Wang, Z. A review of the surveillance techniques for *Aedes albopictus*. *Am. J. Trop. Med. Hyg.* **108**(2), 245–253 (2022).
6. Nascimento, K. L. C., Silva, J. F. M. D., Zequi, J. A. C. & Lopes, J. Comparison between larval survey index and positive ovitrap index in the evaluation of populations of *Aedes (Stegomyia) aegypti* (Linnaeus, 1762) north of Paraná, Brazil. *Environ. Health Insights* **14**, 1178630219886570 (2020).
7. Dritsas, E. & Trigka, M. Remote sensing and geospatial analysis in the big data era: A survey. *Remote Sens.* **17**(3), 550 (2025).
8. Morgan, R. G., Hodgson, M. E., Wang, C. & Schill, S. R. Unmanned aerial remote sensing of coastal vegetation: A review. *Ann. GIS.* **28** (3), 385–399 (2022).
9. Yang, G. et al. Unmanned aerial vehicle remote sensing for field-based crop phenotyping: Current status and perspectives. *Front. Plant Sci.* **8**, 1111 (2017).
10. Zaka, M. M. & Samat, A. Advances in remote sensing and machine learning methods for invasive plant studies: A comprehensive review. *Remote Sens.* **16**, 3781 (2024).
11. Carrasco-Escobar, G. et al. The use of drones for mosquito surveillance and control. *Parasit. Vectors.* **15**(1), 473 (2022).
12. Teillet, C. et al. Characterizing urban landscapes using very-high resolution satellite imagery to predict *Ae. albopictus* larval presence probability in public spaces. *PLoS One.* **20**(11), e0335794 (2025).
13. Wen, D. et al. Change detection from very-high-spatial-resolution optical remote sensing images: Methods, applications, and future directions. *IEEE Geosci. Remote Sens. Mag.* **9**(4), 68–101 (2021).
14. Wong, G. K. & Jim, C. Y. Urban-microclimate effect on vector mosquito abundance of tropical green roofs. *Build. Environ.* **112**, 63–76 (2017).
15. Dom, N. C., Abdullah, N. A. M. H., Dapari, R. & Salleh, S. A. Fine-scale predictive modeling of *Aedes* mosquito abundance and dengue risk indicators using machine learning algorithms with microclimatic variables. *Sci. Rep.* **15**(1), 37017 (2025).
16. Mohd Hardy Abdullah, N. A., Dom, N. C., Pradhan, B., Salleh, S. A. & Dapari, R. Temporal associations between microclimate, adult *Aedes* mosquito indices, and dengue cases at the residence level in Malaysia: Implications for targeted interventions. *PLoS One.* **20**(2), e0316564 (2025).
17. Chen, TH. K., Prishchepov, A. V. & Sabel, C. E. Detecting Urban form Using Remote Sensing: Spatiotemporal Research Gaps for Sustainable Environment and Human Health. In *Earth Data Analytics for Planetary Health. Atmosphere, Earth, Ocean & Space* (Wen, T. H. et al. eds.) 185–217 (Springer Nature, 2023)
18. Milesi, C. & Churkina, G. Measuring and monitoring urban impacts on climate change from space. *Remote Sens.* **12**(21), 3494 (2020).
19. Yang, F. & Chen, L. *High-rise urban form and microclimate* (Springer, 2020).
20. Sureshkumar, S. & Shekhar, S. Impact of urban heat island effect on dengue incidence: A remote sensing approach using thermal and high-resolution optical imagery. *BMC Public Health.* **25**(1), 2914 (2025).
21. Ortiz, D. I., Piche-Ovares, M., Romero-Vega, L. M., Wagman, J. & Troyo, A. The impact of deforestation, urbanization, and changing land-use patterns on the ecology of mosquito and tick-borne diseases in Central America. *Insects* **13** (1), 20 (2021).
22. Marcial-Pablo, M. D. J., Gonzalez-Sanchez, A., Jimenez-Jimenez, S. I., Ontiveros-Capurata, R. E. & Ojeda-Bustamante, W. Estimation of vegetation fraction using RGB and multispectral images from UAV. *Int. J. Remote Sens.* **40** (2), 420–438 (2019).
23. Kakooei, M. & Baleghi, Y. Shadow detection in very high resolution RGB images using a special thresholding on a new spectral–spatial index. *J. Appl. Remote Sens.* **14** (1), 016503–016503 (2020).
24. Mahfodz, Z., Naba, A., Isawasan, P., Osman, M. A. & Dom, N. C. Drone-based composite risk mapping reveals vegetation–shade interaction and housing typology as key determinants of *Aedes* habitat risk. *Sci. Rep.* **16** (1), 5957 (2026).
25. Paladan, S. et al. Unravelling ecological factors influencing phylodynamics of Kyasanur Forest Disease in India. *Infect. Genet. Evol.* **135**, 105831. https://doi.org/10.1016/j.meegid.2025.105831 (2025).
26. Abdullah, N. A. M. H. et al. Spatiotemporal dynamics of dengue hotspots in an urbanizing landscape: a five-year analysis in Selangor, Malaysia. *Clin. Epidemiol. Global Health* **32**, 101966 (2025).
27. Ngugi, H. N. Ecology of immature stages of the dengue fever vector Aedes aegypti (L.) (Diptera: Culicidae) in rural and urban sites of the southern coast of Kenya. (Doctoral dissertation, University of Nairobi). (2023).
28. Kolimenakis, A. et al. The role of urbanisation in the spread of Aedes mosquitoes and the diseases they transmit: A systematic review. *PLoS Negl. Trop. Dis.* **15**(9), e0009631 (2021).
29. Kumar, P. et al. Envisioning urban environments resilient to vector-borne diseases: A protocol to study dengue in Vietnam. *Explor. Digit. Health Technol.* **1** (1), 17–27 (2023).
30. Yeo, H. et al. Dense residential areas promote gene flow in dengue vector mosquito Aedes albopictus. *iScience* **26** (9), 107834 (2023).
31. Murdock, C. C., Evans, M. V., McClanahan, T. D., Miazgowicz, K. L. & Tesla, B. Fine-scale variation in microclimate across an urban landscape shapes mosquito population dynamics and the potential of Aedes albopictus to transmit arboviral disease. *PLoS Negl. Trop. Dis.* **11** (5), e0005640 (2017).
32. Yang, L. et al. Can urban greening increase vector abundance in cities? The impact of mowing, local vegetation, and landscape composition on adult mosquito populations. *Urban Ecosyst.* **22** (5), 827–839 (2019).
33. Robertson, C. Towards a geocomputational landscape epidemiology: Surveillance, modelling, and interventions. *GeoJournal* **82**(2), 397–414 (2017).
34. Fernandez, S. A. et al. Features of the urban environment associated with *Aedes aegypti* abundance in high-rise public apartments in Singapore: An environmental case-control study. *PLoS Negl. Trop. Dis.* **17**(2), e0011075 (2023).
35. Daudé, E., Cebeillac, A., Nakhapakorn, K. & Paul, R. Mapping urban landscapes prone to hosting breeding containers for dengue-vector mosquitoes: A case study in Bangkok. *Urban Sci.* **8**(3), 98 (2024).
36. Andriyani, V., Handoyo, W. & Sayono, S. Arboviral vector dispersal and density in storey buildings: The association of light intensity and air temperature. *Ann. Parasitol.* **68**(4), 727–735 (2022).
37. Maia, L. J. et al. Arbovirus surveillance in mosquitoes: Historical methods, emerging technologies, and challenges ahead. *Experimental Biology and Medicine* **248**(22), 2072–2082 (2023).
38. Dom, N. C. et al. Barriers and opportunities for community engagement in UAV-based dengue management in rural Malaysia. *PLoS One* **20**(4), e0322321 (2025).
39. Mahfodz, Z., Dom, N. C., Salim, H. & Precha, N. *A conceptual framework for assessing the field efficiency of drones in identifying potential breeding sites of the Aedes mosquito* Vol. 17 (International Journal on Sustainable Tropical Design Research & Practice, 2024). 1.
40. Carrasco-Escobar, G. et al. The use of drones for mosquito surveillance and control. *Parasit. Vectors* **15**(1), 473 (2022).
41. Muhmad Kamarulzaman, A. M., Wan Mohd Jaafar, W. S., Mohd Said, M. N., Saad, S. N. M. & Mohan, M. UAV implementations in urban planning and related sectors of rapidly developing nations: A review and future perspectives for Malaysia. *Remote Sens.* **15**(11), 2845 (2023).
42. Tiffin, H. S., Gordon, J. R. & Poh, K. C. One Health, many approaches: Integrated vector management strategies support One Health goals. *Front. Insect Sci.* **5**, 1549348 (2025).

43. Muhmad Kamarulzaman, A. M., Wan Mohd Jaafar, W. S., Mohd Said, M. N., Saad, S. N. M. & Mohan, M. UAV implementations in urban planning and related sectors of rapidly developing nations: A review and future perspectives for Malaysia. *Remote Sens.* **15**(11), 2845 (2023).
44. Khan, A., Gupta, S. & Gupta, S. K. Emerging UAV technology for disaster detection, mitigation, response, and preparedness. *J. Field Robot.* **39** (6), 905–955 (2022).
45. Imran, & Li, J. UAV technology in agriculture: Legal, ethical, and future perspectives. In *UAV Aerodynamics and Crop Interaction: Revolutionizing Modern Agriculture with Drone* 431–462 (Springer Nature Singapore, 2025).
46. Dapari, R. et al. Community participation and technological innovation: Baseline qualitative insights to inform a five-year cohort on drone-based dengue surveillance in Malaysia. *PLoS Negl. Trop. Dis.* **20** (3), e0013979 (2026).
47. Yu, D. Toward integrated urban observatories: Synthesizing remote and social sensing in urban science. *Remote Sens.* **17**(12), 2041 (2025).

Acknowledgements
The authors extend their sincere appreciation to the Faculty of Health Sciences, Universiti Teknologi MARA (UiTM) for providing research facilities, administrative assistance, and access to the institutional drone laboratory essential for field operations. Special thanks are due to the Civil Aviation Authority of Malaysia (CAAM) and the Shah Alam City Council (MBSA) for granting flight permissions and facilitating aerial mapping activities in Seksyen 24, Shah Alam. The authors also acknowledge the Integrated Mosquito Research Group (IMERGE), Faculty of Health Sciences, UiTM, for their technical guidance in spatial data processing, ecological interpretation, and drone-based analytics. This study was conducted in collaboration with the Universitas Brawijaya Adjunct Professor 2025 Program, which provided an academic platform for international research exchange and interdisciplinary collaboration in vector ecology and environmental health. The authors gratefully acknowledge the Vector Control Division, Ministry of Health Malaysia, for their constructive feedback and policy insights that helped align the findings with national dengue surveillance strategies. Appreciation is also extended to the field and laboratory assistants for their commitment to data verification, drone calibration, and site validation. Finally, the authors thank the Research Management Centre (RMC), Universiti Teknologi MARA, for continuous institutional support and for fostering UiTM's commitment to data-driven, sustainable, and globally connected research innovations in public health and vector management.

Author contributions
N.C.D. : Conceptualization, Methodology, Data curation, Formal analysis, Writing – original draft, Writing – review & editing, Supervision. A. N. : Conceptualization, Writing – review & editing, Validation. Z.M.: Conceptualization, Methodology, Writing – original draft, Writing – review & editing. S.A.S.: Data extraction, Visualization, Formal analysis. Pradeep Isawasan: Writing – original draft, Resources. M. A. O.: Writing – review & editing, Project administration.

Funding
This research did not receive any external funding and was fully supported by the internal resources of the Faculty of Health Sciences, Universiti Teknologi MARA (UiTM).

Declarations

Competing interests
The authors declare no competing interests.

Ethical and regulatory compliance
All operations complied with Universiti Teknologi MARA (REC/FSK/2025/001) ethics requirements for environmental and UAV research. Drone missions followed the Civil Aviation Directive CAD 6011 Part XVI (Unmanned Aircraft Systems – Malaysia, 2023) and were approved by both the Civil Aviation Authority of Malaysia (CAAM) and Shah Alam City Council (MBSA).

Additional information
Supplementary Information The online version contains supplementary material available at https://doi.org/10.1038/s41598-026-52556-x.

Correspondence and requests for materials should be addressed to N.C.D.

Reprints and permissions information is available at www.nature.com/reprints.

Publisher's note Springer Nature remains neutral with regard to jurisdictional claims in published maps and institutional affiliations.